Quasiparticle picture for high-harmonic generation in correlated electron systems

Kai Huang[1] and Tao-Yuan Du[1,2,3,*]

[1]*School of Mathematics and Physics, China University of Geosciences, Wuhan 430074, China*

[2]*Hubei Key Laboratory of Optical Information and Pattern Recognition, Wuhan Institute of Technology, Wuhan 430205, China*

[3]*Key Laboratory of Computational Physical Sciences (MOE), Fudan University, Shanghai 200433, China*

(Received 10 May 2023; accepted 4 October 2023; published 16 October 2023)

The key optical and electronic functionalities in condensed materials are determined by the band filling of electrons and their Coulomb correlations. To directly capture how many-body correlations influence the correlated electron dynamics under the driving of laser pulses, the comprehensible quasiparticle picture is desired to distinguish the ultrafast creation and annihilation of doublon-holon pairs in attosecond timescale. Here, we adopt the one-dimensional non-half-filling Hubbard model to study the high-harmonic generation (HHG) in correlated electron systems. As the value of Hubbard U increases, the cutoff energy and spectral features in HHG spectra have been revealed and their scaling laws are explained by the characteristic energy gaps obtained from the electronic bands under the quasiparticle picture. The adjustable degree of band filling in correlated systems paves a way to enhance high-harmonic emissions by regulating the creation of doublon-holon pairs. The complex temporal profile of HHG is elucidated in this work by the light-induced evolution of quasiparticle bands in correlated materials. In addition, the dephasing of the HHG spectrum caused by the vibration-induced disorder or lattice temperature is affirmed in the correlated electron systems and this dephasing process is attributed to quasiparticle-lattice scattering during the doublons and holons propagating among the disordered lattice sites.

DOI: 10.1103/PhysRevB.108.155125

I. INTRODUCTION

High-harmonic generation (HHG) is a highly nonlinear phenomenon resulting from the interaction between intense laser fields and matter [1–3], which has obtained much attention because of its potential for the attosecond light sources and the retrieval of spectrographic information of the electron dynamics underlying generating materials at a subfemtosecond (fs) timescale [4–11]. HHG, initially found in gases [12], has been observed in higher radiation intensity in solids in the past decade, which has garnered much interest, particularly in semiconductors and conductors [3,5,13–28]. Simple semiclassical models for the charge dynamics which lead to this HHG have been proposed for atomic systems, i.e., the so-called three-step model of tunnel ionization, acceleration, and recombination, and have been extended to semiconductors with wide band gap, based on a fixed band structure and the buildup of inter- and intraband electronic currents [29–32].

HHG in semiconductors and semimetals, which are well described by the single-particle band picture, have been investigated intensively. In solid-state HHG, many-body effects in strongly correlated systems have been reported experimentally [33]. Moreover, it has been experimentally observed that the strong Coulomb correlations emerging in the atomically thin WSe_2 shift the optimal timings of recollision by up to 1.2 fs compared to the bulk material [34]. We recognize that the single-active-electron model is inadequate for exploring these phenomena thoroughly, because the strong interaction affects the electron dynamics, which in turn is closely related to HHG. The understanding of the electron-electron correlation effect is lacking but essential for the exploration of HHG and spectroscopic application in correlated materials. So far, the study of HHG in strongly correlated solids has made some progress both theoretically [35–42] and experimentally [33,43]. The Hubbard model has been used to understand the spectroscopic features, but it only captures certain aspects of the physics in real materials [44,45]. Based on the Hubbard model, many aspects affecting HHG in strongly correlated systems have been investigated, such as the spin-charge coupling effect [36], exciton [39], doping [37], dimension [40], correlation strength [35], and electric-field strength [41]. In spite of the great progress that has been made, there are still issues that deserve to be explored in depth. Silva *et al.* found that the lower-order harmonics are suppressed when the Coulomb repulsion U is growing and the spectrographic enhancement region is linear as a function of U [35]. Intriguingly, the spectroscopic dip in the lower-order harmonic region is diminished in two dimensions [40] and non-half-filling band systems [37]. All the above-mentioned spectral features should be explained convincingly.

In addition, the unconventional scaling law for the cutoff energy in HHG spectra implies the electronic structure of correlated materials beyond the single-particle model [35–37,41]. To unravel the spectral feature and its scaling laws, the three-step model formulated in terms of doublon and holon quasiparticles will be involved. Doublons are doubly occupied lattice sites and holons are empty sites. The definition of Mott insulators usually requires the half-filling assumption, in which its Mott gap or minimal energy gap between Hubbard bands characterizes the creation of a doublon-holon pair. The electronic structure and its Mott gap are calculable by

*Corresponding author: duty710@163.com

diagonalizing the system's Hamiltonian, but diagonalization of the entire half-filling system is often not tractable due to memory constraints. The lower degree of band filling is desirable, which is convenient for the theoretical simulations of HHG in correlation materials. Actually, cuprates involve materials in which the highest occupied band is far from the half-filled situation [44]. One can delicately achieve the filling control via the charge doping and gate bias [44,46]. Furthermore, the one-dimensional cuprate chains have also been experimentally synthesized with many different degrees of hole doping [47]. The degree of band filling in cuprate indicates the necessity of studying non-half-filling and is of significance for the many-body dynamics, which is also the concerned issue of this work. Furthermore, it is enlightening to go beyond the assumption of half-filling and to address the impact of band filling on the creation or annihilation of doublon-holon pairs in correlated materials. The quasiparticle-band picture under the single-particle approximation establishes the paradigm to discuss the timing or temporal profile in solid-state harmonic emissions [31]. However, the time-frequency characteristics in HHG from correlated materials are less discussed and the role of the dynamical evolution of quasiparticle bands on the timings of high-harmonic emissions is worth clarifying. For the correlated systems in absence of analytical solutions, the electronic structure can be extracted from the system's spectral function, which is convenient to elaborate our concerned issues.

The paper is organized as follows. In Sec. II, the theoretical methodology and numerical details are introduced. In Sec. III, the obtained results are analyzed and discussed. Finally, in Sec. IV we summarize and conclude. Atomic units are used throughout unless stated otherwise.

II. THEORETICAL MODEL AND METHODS

We adopt the discrete one-dimensional Hubbard model as a paradigmatic model of correlated systems, with periodic boundary conditions. We consider different numbers of electrons, keeping the number of spin-up and -down electrons equal at all times to guarantee spin-neutral situations for a range of growing degrees of band filling. The time-dependent Schrödinger equation (TDSE) includes the electron-electron correlations in the systems interacting with the intense laser field and is denoted as

$$\hat{H}(t) = -t_0 \sum_{s,j=1}^{L} (e^{-i\Phi(t)} c^{\dagger}_{j,s} c_{j+1,s} + e^{i\Phi(t)} c^{\dagger}_{j+1,s} c_{j,s}) + U \sum_{j=1}^{L} c^{\dagger}_{j,\uparrow} c_{j,\uparrow} c^{\dagger}_{j,\downarrow} c_{j,\downarrow}. \quad (1)$$

The electric field $F(t) = -\frac{dA(t)}{dt}$ is related to the time-dependent Peierls phase $\Phi(t) = a_0 A(t)$, in which the lattice constant a_0 is 7.56 a.u. and its amplitude F_0 is 50 MV/cm. This linearly polarized pulse with a wavelength of 9.11 μm ($\omega = 32.9$ THz) has a total duration of ten optical cycles and a $\sin^2$ envelope. We consider the nearest-neighbor hopping term, while $U > 0$ is the on-site Coulomb repulsion. The hopping energy t_0 is set to a constant (0.52 eV) to mimic Sr_2CuO_3 [48]. $c^{\dagger}_{j,s}$ ($c_{j,s}$) is the creation (or annihilation) operator for an electron at site j. $s = (\downarrow, \uparrow)$ labels the spin of the electron. The periodic boundary conditions $c_{j,s} = c_{j+L,s}$ are involved here, where L is the chain length Na_0. Note that the chain length L is $50a_0$ for all non-half-filling cases but is $12a_0$ for the half-filling case.

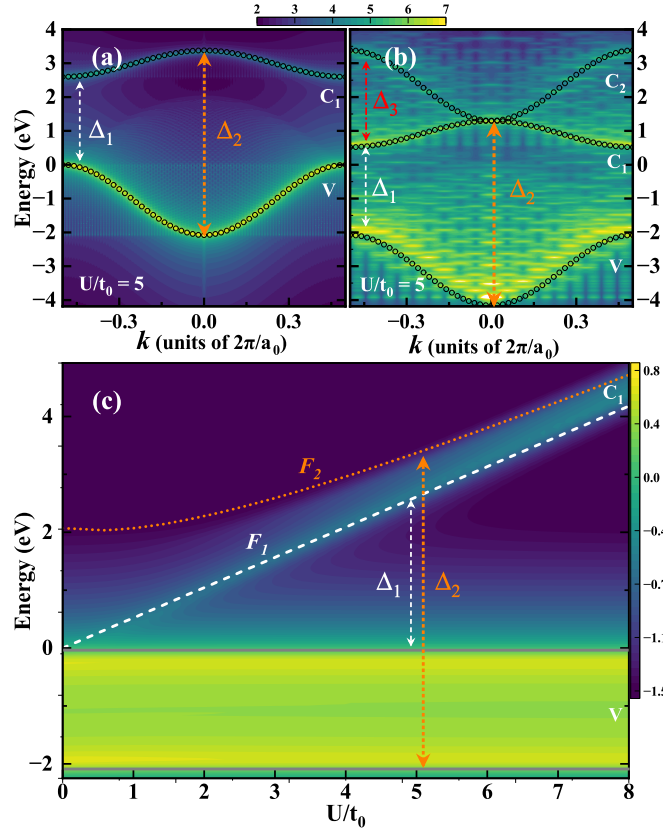

FIG. 1. Quasiparticle-band structures vary with band filling and U/t_0. Panels (a) and (b) respectively show the quasiparticle bands with one- and two-paired electron fillings when the U/t_0 is fixed as 5. (c) Under the case of band filling with one-paired electrons, electronic structures vary with values of U/t_0. V, C_1, and C_2 respectively mark the three energy bands, in which Δ_1, Δ_2, and Δ_3 denote their characteristic energy gaps. In (a) and (b) the analytical dispersions of quasiparticle bands are also presented by dotted curves. In (c) the vertical intervals among F_1 and F_2 lines characterize the U/t_0-dependent bandwidth β of the C_1 band.

To characterize the quasiparticle-band structure in correlated materials varying with U, we expect to obtain the local spectral functions by adopting a large lattice site for a given spin-paired electron. We define the local spectral function of the band structure as $S(k, E) = \sum_n \delta(E - E_n)|\langle k|\varphi_n\rangle|^2$, in which $|\langle k|\varphi_n\rangle|^2 = \sum_j \langle\varphi_{j,n}|e^{-ikja_0} \sum_{j'} e^{ikj'a_0}|\varphi_{j',n}\rangle$. The many-body eigenfunction $|\varphi_n\rangle$ with eigenvalue E_n is obtained from the exact diagonalization method and $|\varphi_{j,n}\rangle$ is the value of eigenfunction $|\varphi_n\rangle$ at the lattice site j. k is the quasimomentum. The field-dressed instantaneous quasiparticle bands can also be obtained from the time-dependent eigenstate $|\varphi_n(t)\rangle$, in which the time-dependent wave function is obtained from the Crank-Nicolson method. The Dirac function is broadened by using a Lorentzian shape $\frac{1}{\pi}\frac{\eta}{(E-E_n)^2+\eta^2}$ with a proper broadening factor $\eta = 0.001t_0$. In Figs. 1(a) and 1(b), we

respectively show the quasiparticle-band structures with one- and two-paired spin electrons, in which the quasiparticle-band dispersions of the lowest two bands are robust. However, the extra spin-paired electrons in Fig. 1(b) characterize one high-lying energy band and the number of spin-paired electrons in the correlated systems would not influence the ultrafast many-body dynamics in the low-energy electronic excitation. Thus we mostly focus on the correlated systems with one-paired spin electrons unless stated otherwise. In addition, for the convenience of discussions, we define a quantity $I(U,E) = \sum_k S(k,E)|_U$ and then display them in Fig. 1(c) to unravel the role of U in the quasiparticle-band structures of the correlated systems. Note that when the U/t_0 is greater than 2, the strongly correlated systems would emerge as multiple Hubbard bands and the formation of the multiple Hubbard bands will be discussed subsequently.

The real space lattice-vibration modes at a specific temperature appear as disordered atomic positions. For establishing the internal connection between lattice vibration and disordered configuration, we develop the finite-temperature crystal model including the electron-electron correlations. Here only a brief description is given. For more details, one refers to Refs. [49–51]. For a lattice chain under a certain temperature, each atomic configuration is a disordered arrangement, which can be depicted by the corresponding radial distribution function. In each disordered configuration, the lattice spacing $\xi_j = x_{j+1} - x_j$ is assumed to obey the standard normal distribution $f(\xi) = (1/\sqrt{2\pi\sigma^2})\exp-[(\xi - a_0)^2/2\sigma^2]$. Since the Coulomb repulsion increases significantly as two nuclei approach each other, intervals between nuclei have a lower limit. Similarly, an upper limit of the nuclear intervals is also necessary before the structural damage. Therefore, for the rationality of our model, a truncated normal distribution generator is adopted and thus only the atomic-pair intervals falling within a range $[a_0 - \xi, a_0 + \xi]$ are retained. Here ξ adopting $a_0/3$ is the maximal deviation under the harmonic-oscillator approximation. The degree of disorder is indicated by the atomic-configuration fluctuation σ, which corresponds to a certain lattice temperature T expressed as $\sigma^2 = \frac{6}{M\omega_D}[\frac{1}{4} + (\frac{T}{\Theta_D})^2\phi]$ [49–52]. Here M is the atomic mass and ω_D is the Debye cutoff frequency. $\Theta_D = \hbar\omega_D/k_B$ is the Debye temperature and $\phi = \int_0^{\Theta_D/T} \theta(e^\theta - 1)^{-1}d\theta$ involves the contribution from all phonon modes described by the phonon density of states [49,50]. In Eq. (1) the hopping energy is a site-independent t_0 under the fixed-nuclear approximation but should satisfy $t_j = t_0\exp[-\frac{x_j - a_0}{\gamma}]$ in the disordered model [53], in which $\gamma = 0.368a_0$.

To compute the HHG spectrum, we first use the electric current operator, defined as

$$\hat{J}(t) = -ia_0t_0\sum_s\sum_{j=1}^{L}(e^{-i\Phi(t)}c^\dagger_{j,s}c_{j+1,s} - \text{H.c.}). \quad (2)$$

Note that, for the disordered case, the parameters a_0 and t_0 in Eq. (1) and Eq. (2) are adjusted as the site-dependent a_j and t_j. All of the 100 configurations included in the disordered situation contribute to the electronic currents, which are coherently summed. The HHG spectrum can be obtained by the Fourier transform of this light-induced total current.

III. RESULTS AND DISCUSSION

A. HHG spectra

We show the HHG spectra as a function of U/t_0 and find the HHG spectra in Figs. 2(a)–2(c) characterize the robust features in the spectroscopic region beyond the 22nd harmonic, even though they are respectively contributed by the band fillings with one-paired, and two-paired and half-filling electrons. In Figs. 2(a) and 2(b) the HHG plateaus obtained from non-half-filling cases reach a great agreement with the half-filling case in 2(c) [35]. When the degree of band filling is growing, one sees that the spectral differences exhibit in the spectral region lowering 22nd harmonic, in which their HHG yields are inhibited, and the underlying mechanism will be discussed below. For highlighting the role of electron-electron correlation in spectral features, in Figs. 2(a)–2(c) two scaling laws (Δ_1 and Δ_2) revealing the spectral enhancement region and the cutoff energies are respectively marked by the white dashed and orange dash-dotted lines. The Mott gap (Δ_{Mott}) marked by an orange dashed line defines the potential barrier for generating the doublon-holon pairs under laser field driving and is associated with the formation of the HHG plateau via the doublon-holon pair annihilation. The electron-electron correlation strength satisfying $U/t_0 > 2$ could form a multiple Hubbard-band system and give rise to high-energy HHG plateaus, while in the case of $U/t_0 < 2$ there are no clear high-energy HHG plateaus in Figs. 2(a) and 2(b).

To elucidate these mentioned spectral features in Fig. 2, we present the U/t_0-dependent quasiparticle-band structures and define their characteristic gaps ($\Delta_{1,2,3}$), as shown in Fig. 1. In spite of the system including electron-electron correlation U in Eq. (1), the spectral functions in Figs. 1(a) and 1(b) display the delicate quasiparticle-band features in crystal momentum k space. For the case with one-paired electrons, the valence band under the tight-binding model can be analytically described as $\text{V}(k) = -\frac{1}{2}\alpha[1 + \cos(ka_0)]$, where $\alpha = 4t_0$ is the width of the valence band [37]. Although the U term is not diagonal in k space and couples different states in the quasiparticle bands, we can fit the local spectral function and also provide a semianalytical energy-band dispersion to unravel the conduction bands. Similarly, the conduction bands are formulated as $\text{C}_1(k) = \frac{1}{2}\beta[1 + \cos(ka_0)] + U$ and $\text{C}_2(k) = -\frac{1}{2}\alpha\cos(ka_0) + U + \beta$, where $\beta = \frac{12t_0^2}{3t_0+U}$ denotes the width of the C_1 band. Here the emergence of the C_2 band in Fig. 1(b) is attributed to the increasing degree of band filling. Note that the absolute energies of bands vary with the degree of band filling, in which the energy level will shift down $4t_0$ for each pair of electrons added. The spectral enhancement region associated with doublon-holon pairs is clarified by the U-dependent gap Δ_1. Moreover, the variation of the maximal energy gap Δ_2 dominates the scaling law of cutoff energy in Fig. 2, as marked by the orange-dotted line in Fig. 1(c). Comparing the spectral enhancement regions under different degrees of band filling, one finds that a recognizable scaling in Fig. 2(a) with one-paired electrons will evolve into a dispersive spectral region in Fig. 2(b). For the situation with two-paired electron filling, the dispersion of the spectral-enhanced region in Fig. 2(b) can be explained by the emergent channel of the elementary charge excitations between C_2 and C_1 bands. The equality relation that Δ_1 plus Δ_3 equals Δ_2

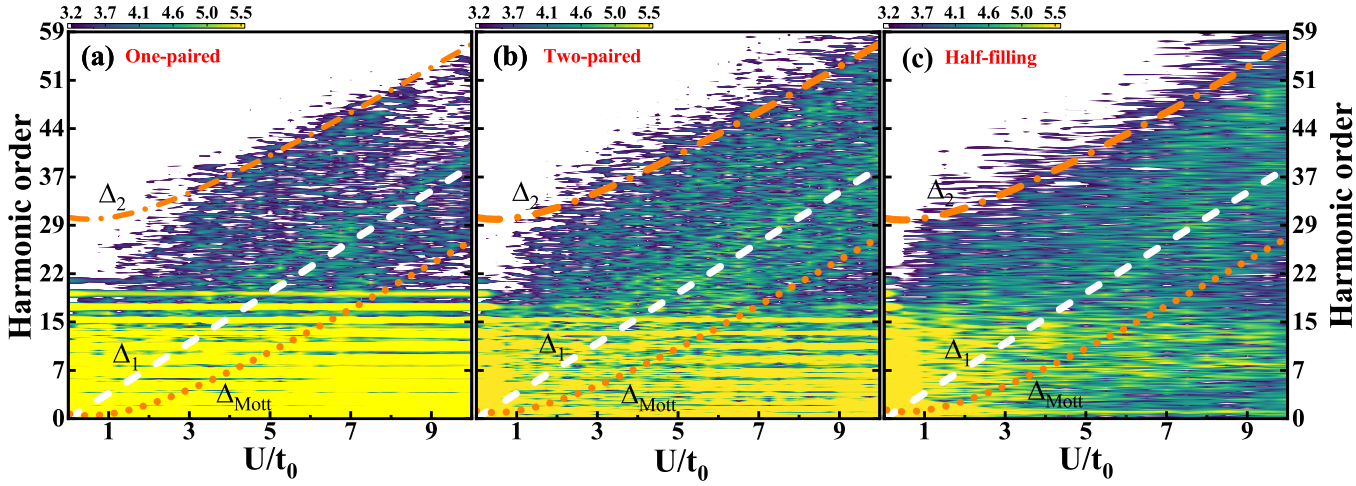

FIG. 2. High-harmonic spectrum as a function of U/t_0. Δ_1 and Δ_2 respectively indicate the spectral enhancement region and cutoff energies. Δ_{Mott} denotes the Mott gap in this correlated material. HHG spectra obtained from cases with one-paired (a), two-paired (b), and half-filling (c) electron filling are presented.

delicately guarantees the robustness of cutoff frequency in Figs. 2(a) and 2(b), which is consistent even in Fig. 2(c) of the half-filling case [35]. Comparing Figs. 2(a)–2(c), one further finds that the lower-order harmonic yields show an inhibition under the growing degree of band filling. Here we will unravel its mechanism. In Fig. 3, the schematic diagram exhibits the hopping manners to create the doublon under different degrees of band filling. In Fig. 3(a) with the lower degree of electron filling, the hopping of the spin-up or spin-down electron is freer. In Fig. 3(b), in contrast, the one spin electron that is adjacent to a doublon would impose a restriction on its hopping behaviors, which is determined by the Pauli exclusion principle and results in the emergence of the high-lying C_2 band in Fig. 1(b). This electronic hopping limitation becomes harsh with the growing number of the filling electron pairs, which could extremely restrain the movement of quasiparticles and thus inhibit the lower-order harmonics emissions. Note that this electronic-hopping restraint in situations with two or three dimensions could be relieved to some extent, which could be verified by the absence of spectral dip in lower-order harmonics in the reported works [40,41,54]

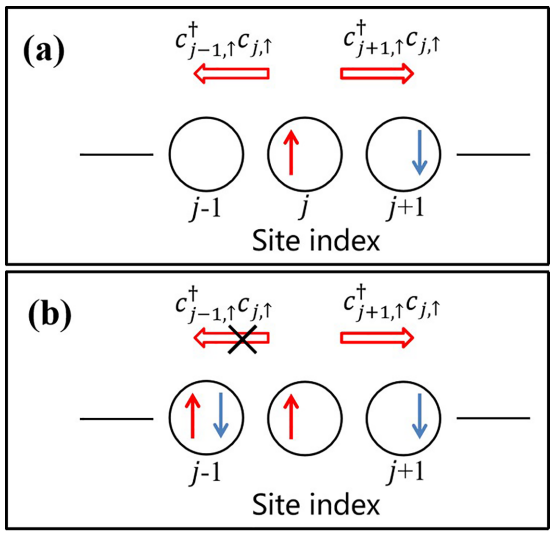

FIG. 3. Schematic diagram for the creation of doublon-holon pairs under different degrees of band filling. A red arrow indicates that a spin-up electron occupies the given site; similarly, a blue arrow indicates that a spin-down electron occupies the given site. The allowable transition directions are denoted by operators written at the top of each panel.

Next we turn to discussing the scaling laws as a function of the field strength. For the different degrees of band filling, we show their HHG spectra as a function of the electric-field amplitude, as presented in Figs. 4(a)–4(c). For the non-half-filling cases in Figs. 4(a) and 4(b), the cutoff frequency as a function of the field strength presents a linear law ($\Omega = U + mF_0$) and is finally restrained by the maximal band gap Δ_2. Here m denotes the site number of Wannier-Stark ladders, in which the HHG originates from transitions among them [41]. In contrast to that, in Fig. 4(c) the cutoff frequency under the half-filling situation exhibits the field-independent characteristic. The linear scaling law of the cutoff frequency in non-half-filling cases can be attributed to the many-body dynamic of the creation and annihilation of the doublon-holon pairs. As mentioned in Fig. 3, in the lattice chain with the lower degree of electron filling the movement of quasiparticles is less restrained. Thus the cutoff frequency is determined by the coherent movement displacement of the doublon-holon pair, which gives rise to the linear law in Figs. 4(a) and 4(b). In the half-filling system, the excitation and recombination of the doublon-holon pair are extremely localized. Thus the first allowable excitations have energies between Δ_1 and Δ_2, which intrinsically dominates the harmonic emission in this spectral range. When the electric-field amplitude is above 10 MV/cm, the Mott band gap Δ_{Mott} could be formed, as presented in the subsequent Fig. 5(a), and the threshold for the transition is crossed. Figure 4(c) verifies the fact that the range of emitted harmonic energies and the cutoff frequency are field independent. Here, Fig. 4(c) suggests that harmonic emission is contributed by one-photon transitions back to the original valence state via a single doublon-holon pair annihilation [35].

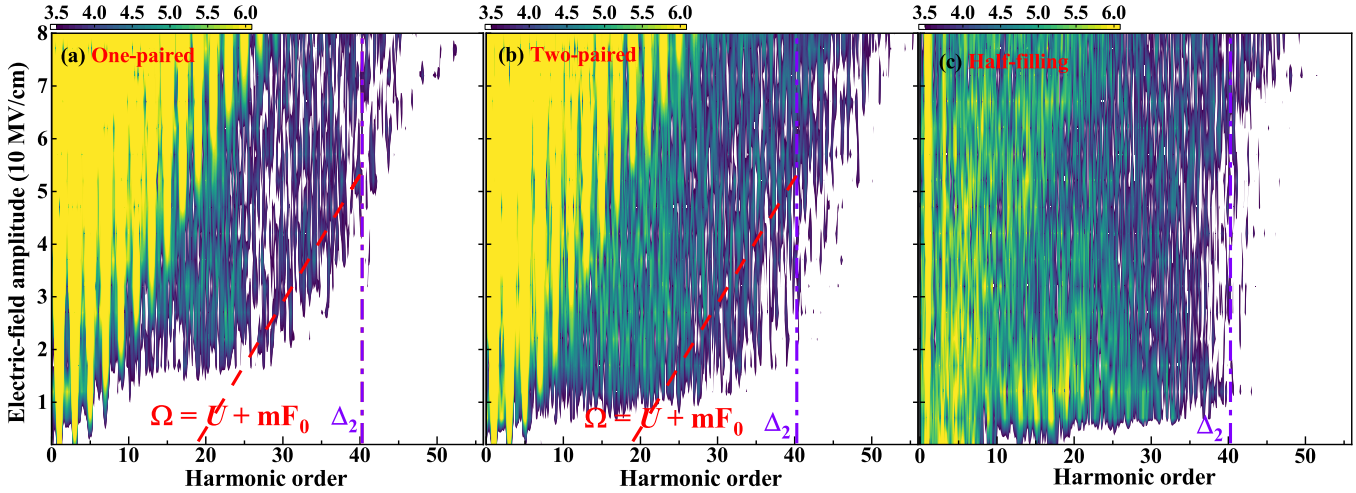

FIG. 4. High-harmonic spectrum as a function of the electric-field amplitude F_0. Δ_2 indicates the maximum band gap. For given $U/t_0 = 5$, HHG spectra obtained from cases with one-paired (a), two-paired (b), and half-filling (c) electron filling are presented.

B. Time-resolved high-harmonic emission

High-harmonic spectroscopy provides a way to resolve the many-body ultrafast dynamics. Here we will discuss the temporal profiles of the quantum trajectory in HHG of correlated materials. Taking $U/t_0 = 5$ as a representative example, the strongly correlated systems driven by the laser fields exhibit the dynamical evolution of quasiparticle bands. In Fig. 5(a), we observe two characteristic situations in the instantaneous quasiparticle-band structures and the evolution of two energy bands undergoes their respective flips. The field-free valence band is first deformed as V^{I} and then completes its flip shown as V^{II}, while the conduction band (C_1) first achieves its flip (C_1^{I}) and then regains the original dispersion (C_1^{II}). Note that the whole evolution process is done in each optical cycle. In Fig. 5(a), we confirm the Mott gap ($\Delta_{\text{Mott}} = \Delta_2 - 2\alpha$), where an instantaneous minimal gap between V^{II} and C_1^{II} bands is formed at $k = 0$. The characteristic gaps involved in the instantaneous band structure can be verified by the HHG spectrum shown in Fig. 5(b). In other words, the high-harmonic spectroscopy paves a promising route to probe the light-induced quasiparticle band in the quantum materials. Then we further perform the time-frequency analysis on this HHG spectrum and obtain an intricate temporal profile, as presented in Fig. 5(c). To distinguish the quantum trajectories reflecting the recombination of doublon-holon pairs, we make the semiclassical predictions under the quasiparticle-band picture. For the instantaneous energy bands shown in Fig. 5(a), their group velocities of doublons and holons in the real space can be written as $v_n^g(k) = \dot{x} = \frac{\partial E_n(k)}{\partial k}|_k$, where E_n is the above-mentioned quasiparticle-band dispersion of doublons or holons in k space. Under the drive of the laser fields, the doublon and holon propagate with their respective group velocities $v_n^g(n = d, h)$. The high-order harmonics with band gap energy would be emitted when the doublon-holon recombination occurs in real space. Here, the relative displacement between doublon and holon is denoted as $\Delta x =$

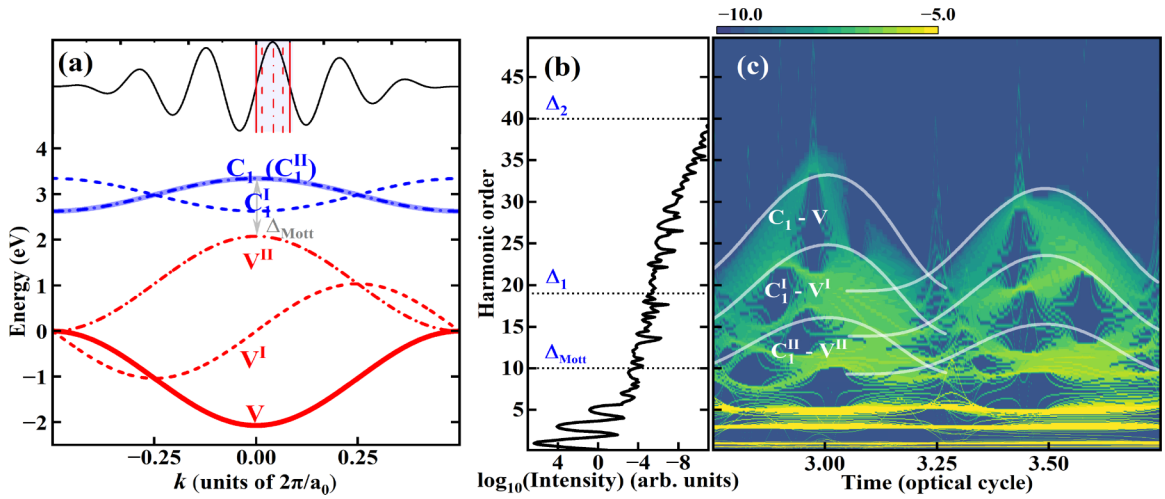

FIG. 5. (a) Instantaneous quasiparticle-band structures in correlated systems, (b) the corresponding HHG spectrum, and (c) its time-frequency analysis. Δ_{Mott} is the Mott gap specified in (a). The laser pulse has a duration of six optical cycles and electric-field amplitude $F_0 = 10$ MV/cm. Three characteristic times in the top panel of (a) are specified.

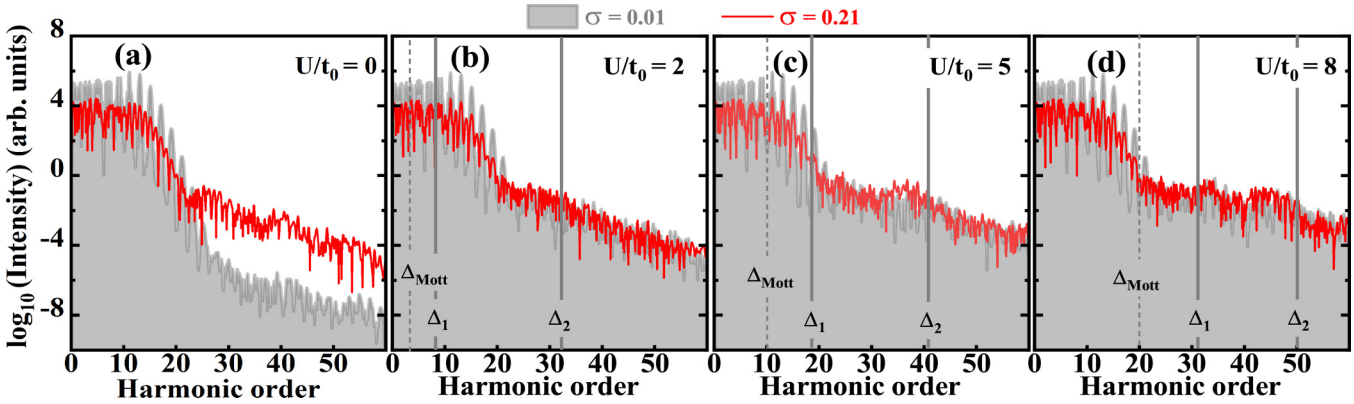

FIG. 6. Panels[(a)–(d)] exhibit the disorder effect in HHG with the growing strength of electron-electronic correlation. The gray background curves and red solid curves respectively denote the HHG spectra under the cases of $\sigma = 0.01$ and 0.21 a.u. The vertical lines in [(b)–(d)] denote the characteristic gaps in their quasiparticle-band structures of the correlated materials.

$\int_{t'}^{t}\{v_d^g[k(\tau)] - v_h^g[k(\tau)]\}d\tau$, where Δx represents the relative displacement of doublon and holon from ionization moment t' to recombination moment t. The condition of high-harmonic emission satisfies the zero displacement in the recombination step, which is called the closed-trajectory model [29]. In Fig. 6, the harmonic emissions beyond Δ_2 can be unraveled by the open-trajectory model involving the quantum coherence of wave function [42,51]. To further unravel the underlying many-body dynamics in the HHG spectrum, in Fig. 5(c) we show the charge dynamics and also clarify their semiclassical trajectories of the doublon-holon recombination. The comparison between curves and the color map in Fig. 5(c) reveals that, based on the field-free C_1 and V bands, its semiclassical predictions only confirm the quantum trajectories within the 19th–40th harmonics, specifically in the spectral region (Δ_1-Δ_2). However, in Fig. 5(c) the spectral region ranging from Δ_{Mott} to Δ_1 cannot be explained without the field-dressed quasiparticle bands, i.e., C_1^{I}-V^{I} and C_1^{II}-V^{II}. Keeping the envelope of laser pulse in mind, the instantaneous quasiparticle bands will be to some extent different between the adjacent half cycles. In addition, the quantum trajectories contributed by doublon-holon pair recombination should involve the dynamical quasiparticle bands, but we only involve the instantaneous bands at three characteristic timings marked in the top panel of Fig. 5(a). All the factors mentioned above lead to the deviation between semiclassical and quantum trajectories, as shown in Fig. 5(c). However, the essence of temporal emission trajectories has been clarified.

C. Vibration-induced disorder or lattice temperature effect

The real-space lattice vibration at a specific temperature appears as the disordered atomic arrangement. The degree of disorder is determined by the growing lattice temperature induced by the laser-field radiation. Thus the disorder or temperature effect is an additional degree of freedom to control the HHG in correlated electron systems. In Fig. 6, we investigate the U-dependent HHG spectra varying with the disordered degree. Generally, the correlation-free and single-band electron systems driven by the laser field could not generate the HHG plateau, because only the intraband movement of the charge carrier is involved. In Fig. 6(a), an extremely weak disorder ($\sigma = 0.01$ a.u.) in the correlation-free system produces the distinct HHG plateau and this HHG plateau is further enhanced under the case with the growing disordered degree ($\sigma = 0.21$ a.u.). In other words, for the weakly correlated case ($U/t_0 \leqslant 2$), the disordered degree only dominates the formation and enhancement of the HHG plateau and the influence of the disordered degree is diminished when the U/t_0 value is greater than 2, as presented in Figs. 6(b), 6(c), and 6(d). Furthermore, for these cases with the strong electron-electron correlations, the growing value of U/t_0 always promotes the harmonic yields around Δ_1 whether this system includes the structural disorder or not.

To clarify the role of structural disorder on the HHG plateau, in Figs. 7(b1)–7(b4) we make an insight into the quasiparticle-band structure varying with disordered degree and U/t_0. The disorder resulting from lattice vibration does not destroy the main characteristics of its energy band but could perturb the quasiparticle-band structure. This perturbation gives rise to the disorder-induced complex bands, in which a single band in Figs. 7(b1) and 7(b2) becomes the multiple-Hubbard band system including many subbands. Thanks to these disorder-induced subbands, the excitation rate is high around the minimum band gaps (avoided level crossings). In Fig. 7(a), the formation and the enhanced yield of the HHG plateau are attributed to the high excitation rate among these disorder-induced subbands. In contrast to the subband system induced by the structural disorder, one whole and high-lying Hubbard band is gradually formed when the ratio of U/t_0 is larger than 2, as presented in Figs. 7(a1)–7(a4). Considering the fact that the multiple Hubbard band system is formed under the case with sufficiently correlated strength, the recombination of doublon-holon pairs can occur in the strongly correlated systems. Thus, in Figs. 6(b), 6(c), and 6(d), the diminished influence of the disordered degree in HHG spectra is readily comprehensible and the characteristic gaps varying with correlated electron strength are delicately reflected by their respective HHG spectra.

Most important of all, for the vibration-induced disordered systems, one can observe that the high harmonics below the Mott gap are suppressed whether or not the electron correlation is involved, as shown in Fig. 6. In HHG spectra

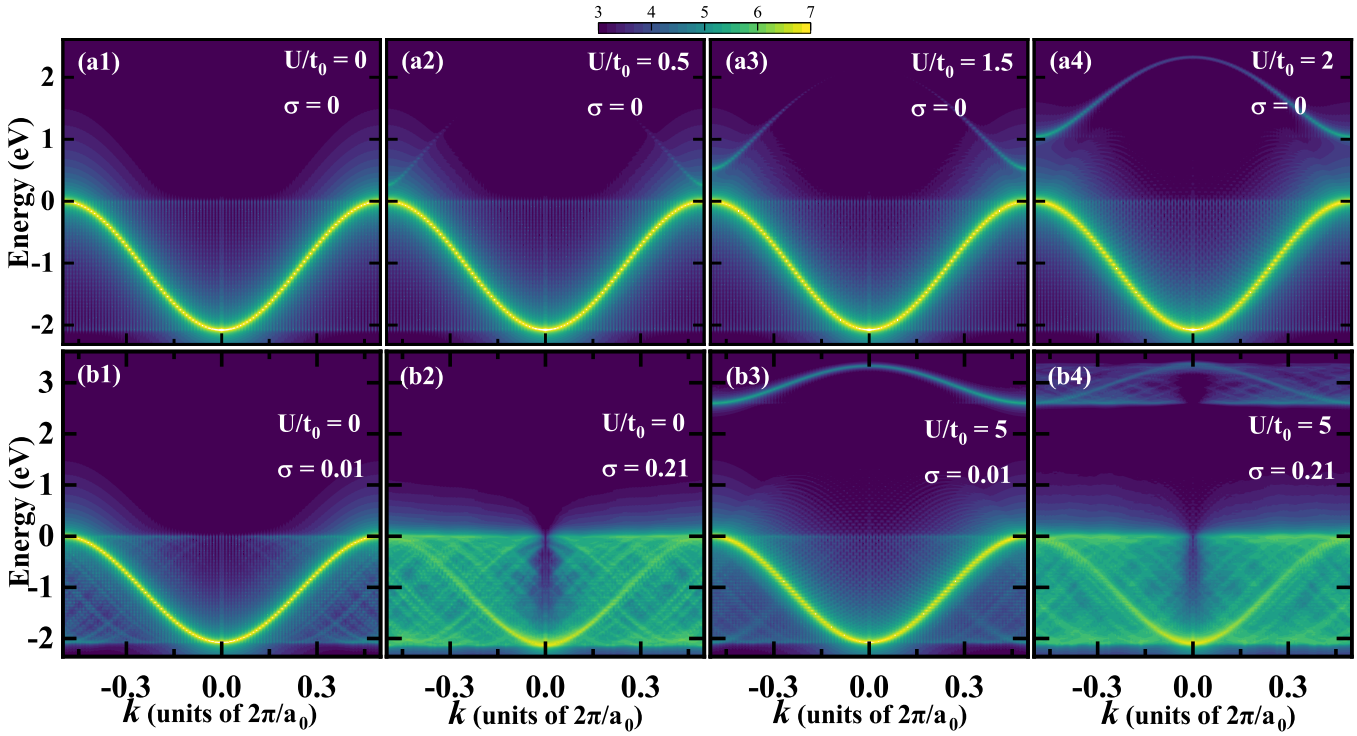

FIG. 7. Panels [(a1)–(a4)] present the evolution and formation of the conduction band C_1 when the strength of electron-electron correlation is increasing. Panels (b1) and (b2) show the impact of the disordered degree on the energy bands under the correlation-free case, while (b3) and (b4) display the influence of disorder in this system with strongly correlated interaction.

this decoherence varying with disordered degrees or lattice temperatures had been first verified in the single-electron case [51]. Note that this temperature dependence of HHG is also discussed under the mechanism of spin-charge coupling [33,36]. Essentially, the lower orders of high harmonics are usually determined by the intraband dynamics, i.e., the movement of doublons or holons. Its underlying mechanism of dephasing is attributed to each quasiparticle-lattice scattering occurring among the disordered lattice sites, which has a significant effect on the temperature-dependent HHG spectra. The temperature-dependent scaling in high-harmonic spectroscopy could make a calibration on the time resolution of correlated electron dynamics.

IV. SUMMARY AND CONCLUSION

To summarize, we study the cases with doping away from the half-filling situation and assess their HHG spectra varying with the degree of band filling in strongly correlated materials. As the growing strength of electron-electron correlation, the HHG plateau is enhanced in the weakly correlated case ($U/t_0 \leqslant 2$) and a spectral enhancement region around the minimal gap Δ_1 emerges in the strongly correlated case ($U/t_0 > 2$). The yields of the lowest harmonic orders are suppressed when the degree of band filling is gradually growing from the one- or two-paired to half-filling cases. These spectral features attributed to the variation of hopping behaviors are the observable signatures of the sensitive, ultrafast response of many-body correlated dynamics to extreme nonperturbative driving of the laser field. In dealing with the numerical simulation of the Hubbard model, some approximations such as the lattice size and dimensionality are introduced, in which the desired quasiparticle-band picture provides a means to assess the temporal profile in the correlated creation-annihilation dynamics of doublon-holon pairs. Furthermore, the field-driving evolution of instantaneous quasiparticle-band structure in correlated materials can be elucidated clearly under the quasiparticle picture via the temporal resolution of high-harmonic emissions. The evolution of the instantaneous band structures is of significance for understanding the electric and optical properties in correlated systems. Keeping the recent temperature-dependent HHG spectra in mind, we clarify here the vibration-induced disorder (or lattice temperature) effect on the HHG spectrum from non-half-filling correlated systems. This work verifies the mechanisms of quasiparticle-lattice scatterings in correlated systems, which gives an alternative viewpoint to interpreting the temperature-dependent HHG experiments.

ACKNOWLEDGMENTS

This work is supported by the Natural Science Foundation of Hubei Province China (Grant No. 2023AFB613), the Fundamental Research Funds for the Central Universities, China University of Geosciences (Wuhan) with Grant No. G1323523064, and the Project of Hubei Key Laboratory of Optical Information and Pattern Recognition, Wuhan Institute of Technology.

[1] M. Lewenstein, P. Balcou, M. Y. Ivanov, A. L'Huillier, and P. B. Corkum, Phys. Rev. A **49**, 2117 (1994).
[2] M. Lein and J. M. Rost, Phys. Rev. Lett. **91**, 243901 (2003).
[3] S. Ghimire, A. D. DiChiara, E. Sistrunk, P. Agostini, L. F. DiMauro, and D. A. Reis, Nat. Phys. **7**, 138 (2011).
[4] F. Krausz and M. Ivanov, Rev. Mod. Phys. **81**, 163 (2009).
[5] O. Schubert, M. Hohenleutner, F. Langer *et al.*, Nat. Photon. **8**, 119 (2014).
[6] W. Li, X. Zhou, R. Lock, S. Patchkovskii, A. Stolow, H. C. Kapteyn, and M. M. Murnane, Science **322**, 1207 (2008).
[7] M. Lein, N. Hay, R. Velotta, J. P. Marangos, and P. L. Knight, Phys. Rev. A **66**, 023805 (2002).
[8] R. Torres, N. Kajumba, J. G. Underwood *et al.*, Phys. Rev. Lett. **98**, 203007 (2007).
[9] P. M. Kraus, B. Mignolet, D. Baykusheva *et al.*, Science **350**, 790 (2015).
[10] T. T. Luu and H. J. Wörner, Nat. Commun. **9**, 916 (2018).
[11] T. Brabec and F. Krausz, Rev. Mod. Phys. **72**, 545 (2000).
[12] M. Ferray, A. L'Huillier, X. F. Li, L. A. Lompre, G. Mainfray, and C. Manus, J. Phys. B: At., Mol., Opt. Phys. **21**, L31 (1988).
[13] T. T. Luu, M. Garg, S. Y. Kruchinin, A. Moulet, M. T. Hassan, and E. Goulielmakis, Nature (London) **521**, 498 (2015).
[14] G. Vampa, T. J. Hammond, N. Thire, B. E. Schmidt, F. Legare, C. R. McDonald, T. Brabec, and P. B. Corkum, Nature (London) **522**, 462 (2015).
[15] F. Langer, M. Hohenleutner, C. P. Schmid, C. Pöllmann, P. Nagler, T. Korn, C. Schüller, M. Sherwin, U. Huttner, J. Steiner, S. Koch, M. Kira, and R. Huber, Nature (London) **533**, 225 (2016).
[16] M. Hohenleutner, F. Langer, O. Schubert, M. Knorr, U. Huttner, S. Koch, M. Kira, and R. Huber, Nature (London) **523**, 572 (2015).
[17] G. Ndabashimiye, S. Ghimire, M. Wu, D. A. Browne, K. J. Schafer, M. B. Gaarde, and D. A. Reis, Nature (London) **534**, 520 (2016).
[18] H. Liu, Y. Li, Y. S. You, S. Ghimire, T. F. Heinz, and D. A. Reis, Nat. Phys. **13**, 262 (2017).
[19] Y. S. You, D. A. Reis, and S. Ghimire, Nat. Phys. **13**, 345 (2017).
[20] N. Yoshikawa, T. Tamaya, and K. Tanaka, Science **356**, 736 (2017).
[21] K. Kaneshima, Y. Shinohara, K. Takeuchi, N. Ishii, K. Imasaka, T. Kaji, S. Ashihara, K. L. Ishikawa, and J. Itatani, Phys. Rev. Lett. **120**, 243903 (2018).
[22] N. Yoshikawa, K. Nagai, K. Uchida, Y. Takaguchi, S. Sasaki, Y. Miyata, and K. Tanaka, Nat. Commun. **10**, 3709 (2019).
[23] B. Cheng, N. Kanda, T. N. Ikeda, T. Matsuda, P. Xia, T. Schumann, S. Stemmer, J. Itatani, N. P. Armitage, and R. Matsunaga, Phys. Rev. Lett. **124**, 117402 (2020).
[24] J. Li, X. Zhang, S. Fu, Y. Feng, B. Hu, and H. Du, Phys. Rev. A **100**, 043404 (2019).
[25] T.-Y. Du, Opt. Lett. **46**, 2007 (2021).
[26] M. Lysne, Y. Murakami, and P. Werner, Phys. Rev. B **101**, 195139 (2020).
[27] Y. Murakami, S. Takayoshi, A. Koga, and P. Werner, Phys. Rev. B **103**, 035110 (2021).
[28] C. Ma, X.-B. Bian, and T.-Y. Du, Phys. Rev. B **106**, 125117 (2022).
[29] P. B. Corkum, Phys. Rev. Lett. **71**, 1994 (1993).
[30] D. Golde, T. Meier, and S. W. Koch, Phys. Rev. B **77**, 075330 (2008).
[31] G. Vampa, C. R. McDonald, G. Orlando, D. D. Klug, P. B. Corkum, and T. Brabec, Phys. Rev. Lett. **113**, 073901 (2014).
[32] G. Wang and T.-Y. Du, Phys. Rev. A **103**, 063109 (2021).
[33] K. Uchida, G. Mattoni, S. Yonezawa, F. Nakamura, Y. Maeno, and K. Tanaka, Phys. Rev. Lett. **128**, 127401 (2022).
[34] J. Freudenstein, M. Borsch, M. Meierhofer, D. Afanasiev, C. P. Schmid, F. Sandner, M. Liebich, A. Girnghuber, M. Knorr, M. Kira, and R. Huber, Nature (London) **610**, 290 (2022).
[35] R. E. F. Silva, I. V. Blinov, A. N. Rubtsov, O. Smirnova, and M. Ivanov, Nat. Photon. **12**, 266 (2018).
[36] Y. Murakami, K. Uchida, A. Koga, K. Tanaka, and P. Werner, Phys. Rev. Lett. **129**, 157401 (2022).
[37] T. Hansen and L. B. Madsen, Phys. Rev. B **106**, 235142 (2022).
[38] G. McCaul, C. Orthodoxou, K. Jacobs, G. H. Booth, and D. I. Bondar, Phys. Rev. Lett. **124**, 183201 (2020).
[39] M. Udono, K. Sugimoto, T. Kaneko, and Y. Ohta, Phys. Rev. B **105**, L241108 (2022).
[40] C. Orthodoxou, A. Zaïr, and G. H. Booth, npj Quantum Mater. **6**, 76 (2021).
[41] Y. Murakami, M. Eckstein, and P. Werner, Phys. Rev. Lett. **121**, 057405 (2018).
[42] Y. Wang, M. Claassen, B. Moritz, and T. P. Devereaux, Phys. Rev. B **96**, 235142 (2017).
[43] M. R. Bionta, E. Haddad, A. Leblanc, V. Gruson, P. Lassonde, H. Ibrahim, J. Chaillou, N. Émond, M. R. Otto, A. Jiménez-Galán, R. E. F. Silva, M. Ivanov, B. J. Siwick, M. Chaker, and F. Légaré, Phys. Rev. Res. **3**, 023250 (2021).
[44] M. Imada, A. Fujimori, and Y. Tokura, Rev. Mod. Phys. **70**, 1039 (1998).
[45] P. A. Lee, N. Nagaosa, and X.-G. Wen, Rev. Mod. Phys. **78**, 17 (2006).
[46] K. S. Novoselov, A. K. Geim, S. V. Morozov, D. Jiang, Y. Zhang, S. V. Dubonos, I. V. Grigorieva, and A. A. Firsov, Science **306**, 666 (2004).
[47] Z. Chen, Y. Wang, S. N. Rebec, T. Jia, M. Hashimoto, D. Lu, B. Moritz, R. G. Moore, T. P. Devereaux, and Z.-X. Shen, Science **373**, 1235 (2021).
[48] T. Oka, Phys. Rev. B **86**, 075148 (2012).
[49] I. K. Jeong, R. H. Heffner, M. J. Graf, and S. J. L. Billinge, Phys. Rev. B **67**, 104301 (2003).
[50] D. Schlesinger, K. Thor Wikfeldt, L. B. Skinner, C. J. Benmore, A. Nilsson, and L. G. M. Pettersson, J. Chem. Phys. **145**, 084503 (2016).
[51] T.-Y. Du and C. Ma, Phys. Rev. A **105**, 053125 (2022).
[52] P. Debye, Ann. Phys. (NY) **344**, 789 (1912).
[53] C. Jürß and D. Bauer, Phys. Rev. B **99**, 195428 (2019).
[54] T.-Y. Du, Phys. Rev. A **104**, 063110 (2021).